Synthesis and characterization of a novel alkali mixed magnesium-aluminum phosphate with a layered structure - $KMgAl(PO_4)_2$

Ines Mokni,[a] Abdessalem Badri,[a,*] Sami Slimi,[b,c] Karim Omri,[d] Pavel Loiko,[e] Rosa Maria Solé,[b] Magdalena Aguiló,[b] Francesc Díaz,[b] Xavier Mateos,[b,#] and Mongi Ben Amara[a]

[a]*Laboratory of Interfacial and Advanced Materials, Faculty of Sciences, University of Monastir, 5000 Monastir, Tunisia*

[b]*Universitat Rovira i Virgili (URV), Física i Cristal·lografia de Materials i Nanomaterials (FiCMA-FiCNA), Marcel.li Domingo 1, 43007 Tarragona, Spain, # Serra Húnter Fellow*

[c]*I.P.E.I. of Monastir, Unit of Materials and Organic Synthesis, 5019 Monastir, UR17ES31, Tunisia*

[d] *Physics Laboratory of Nanomaterials for Environment, University of Gabes, 6072 Gabes, Tunisia*

[e]*Centre de Recherche sur les Ions, les Matériaux et la Photonique (CIMAP), UMR 6252 CEA-CNRS-ENSICAEN, Université de Caen Normandie, 6 Boulevard Maréchal Juin, 14050 Caen Cedex 4, France*

*Corresponding author: badri_abdessalem@yahoo.fr

Address: Laboratory of Interfacial and Advanced Materials, Faculty of Sciences, University of Monastir, 5000 Monastir, Tunisia. Tel: (216) 73 500 280. Fax: (216) 73 500 278

Abstract: A novel phosphate compound - potassium magnesium-aluminum double phosphate with chemical formula $KMgAl(PO_4)_2$ - has been synthesized. Platelet-shaped single crystals have been grown from the flux using $K_2Mo_2O_7$ as a solvent. The powder form has been obtained through a sol-gel reaction. It has been characterized by X-ray diffraction, SEM, FTIR and UV-Vis-DR, as well as electronic structure calculations. $KMgAl(PO_4)_2$ crystallizes in the trigonal centrosymmetric space group $P\bar{3}m1$ (No. 164) with unit cell parameters $a = b = 5.347(1)$ Å, $c = 7.903(10)$ Å, $\gamma = 120°$ (Z = 1). The main characteristic of the crystal is the two-dimensional (2D) lamellar framework formed by $Mg|AlO_4$ and PO_4 tetrahedrons sharing their vertices of oxygen atoms, with the K^+ cations located within the interlayer space. The sample morphology and chemical composition were revealed by the SEM-EDX analysis. The IR spectroscopy of $KMgAl(PO_4)_2$ confirmed the existence of a single PO_4 group in agreement with the structural study. A relatively large indirect band gap of 3.86 eV was determined.

Keywords: Complex phosphates; layered structure; electronic structure; optical properties.

1. Introduction

Inorganic phosphates constitute an important class of materials, which have received widespread interest in recent years. They have been deeply studied regarding their structural diversity originating from the way in which the P-O phosphate group associates with an alkali or alkaline rare-earth ion (A) and / or a metal ion (M) to form a stable AMPO oxide. Hence, dissimilar crystalline structure has been engendered a two-dimensional (2D) layer or a three-dimensional (3D) framework with hexagonal, rectangular, or triangular tunnels containing the alkali cations. These frameworks can be either purely tetrahedral (PO_4 / MO_4) or made up of several types of polyhedrons (e.g., PO_4 / MO_4, MO_5 or MO_6) especially in the case of M adopting several coordinations ranging from four to six, such as in the case of iron and aluminum in oxides [1, 2, 3].

Aluminum phosphates find potential applications as ionic conductors [4, 5, 6], optical materials [7] and catalyzers [8, 9, 10]. Lithium aluminum titanium phosphate ($Li_{1.3}Al_{0.3}Ti_{1.7}(PO_4)_3$, LATP) which can be synthesized by different methods has been widely studied due to its high density and an ionic conductivity of 1.88×10^{-4} $S\cdot cm^{-1}$ at room-temperature [11]. Other compounds such as $Rb_3Al_2(PO_4)_3$ and $K_3Al_2(PO_4)_3$ [12] appeared as promising materials for second harmonic generation with efficiencies comparable to that of KH_2PO_4 (KDP). Regarding luminescent materials, $Na_3Al_2(PO_4)_3$ doped with Ce^{3+} ions exhibited a broadband UV emission at 328 nm [13] while under doping with Eu^{3+} and Mn^{2+}, it gave rise to emissions in the red and green spectral ranges, at 615 nm and 515 nm, respectively. The $(NH_4)_3Al_2(PO_4)_3$ and $Al_2(PO_4)_2(OH)_2(NH_4)_{2-x}(H_3O)_x$ compounds [14] were proved to be of interest as selective and active heterogeneous solid catalysts for the Friedel-Crafts acylation and acetalization reactions. These catalysts were found to be stable, and they could be recycled more than four times without significant loss of reactivity.

Recently, the $AM^{II}Al(PO_4)_2$ system, where A is an alkali cation and M^{II} is a transition metal, has been studied with several reported compounds. They are classified depending on their structural type based on the metal coordination (six or four). The $KCuAl(PO_4)_2$ [15] and $RbCuAl(PO_4)_2$ [16] compounds exhibit 3D structures formed by CuO_6 octahedrons sharing a common edge to form zigzag chains connected to a AlO_5 polyhedron and PO_4 tetrahedrons through corners and an edge. The compounds $KCoAl(PO_4)_2$ [17], $NH_4(Al,Co)_2(PO_4)_2$ [18], $KZnAl(PO_4)_2$ and β-$NaZnAl(PO_4)_2$ [19], $(NH_4)_{0,83}(Zn_{0,83}Al_{1,17})(PO_4)_2$ [20] and α-$NaZnAl(PO_4)_2$ [21] adopted a 3D structural framework formed entirely by tetrahedrons.

In the present work, we report on the synthesis and characterization of a novel compound within the $AM^{II}Al(PO_4)_2$ system owing to the relevance of this phosphate family of materials, in particular, potassium magnesium aluminum phosphate, $KMgAl(PO_4)_2$.

2. Experimental

Single crystals of $KMgAl(PO_4)_2$ have been grown from the flux with potassium dimolybdate $K_2Mo_2O_7$ as a solvent with an atomic ratio P:Mo = 1:2. Appropriate amounts of KNO_3 (purity: 99%), $Mg(NO_3)_2\cdot6H_2O$ (98.5%), $Al(NO_3)_3\cdot9H_2O$ (99%), $(NH_4)_2HPO_4$ (99%) and $(NH_4)_6Mo_7O_{24}\cdot4H_2O$ (99%) were dissolved in an acidulate solution. The obtained solution was

evaporated to dryness at 100 °C. The resulting dried residue was ground in an agate mortar to get a homogenous mixture and progressively heated in a platinum crucible between 200 °C and 600 °C to release H_2O, NH_3 and NO_2 gases. Then, it was reground, melted for 1 h at 1150 °C and subsequently cooled at a rate of 10 °C/h down to 600 °C before switching off the furnace. After being boiled in water to dissolve the flux, colorless crystals were extracted.

The powder form was prepared by sol-gel reaction in air using stoichiometric amounts of the KNO_3, $Mg(NO_3)_2{\cdot}6H_2O$, $Al(NO_3)_3{\cdot}9H_2O$ and $(NH_4)_2HPO_4$ reagents. At first, these reagents were dissolved in an acidulate solution, followed by an addition of citric acid (CA) to engender the complexation of the metal cations. After that, appropriate amounts of ethylene glycol (EG) were added (the EG:CA molar ratio was 1:1) to obtain a gel. The gel became a resin after heating at 80 °C for 1 h. During continued heating at 140–150 °C for 1 h, the solution became more and more viscous and finally became a xerogel. To complete drying, the xerogel was calcined at 250 °C for 1 h. The resulting powder was heated in a furnace at 400–600 °C for 12 h using a platinum crucible, and then was cooled down to room temperature. The resulting mixture was ground in an agate mortar to give a homogenous material and finally annealed at 1050 °C for 12 h, after which the furnace was turned off and a fine white powder was obtained.

The structure and the phase purity of the synthesized powder sample was examined using a Philips X'Pert automated diffractometer with Ni-filtered Cu-Kα radiation (λ = 1.5406 Å). The chemical composition and the morphology were revealed by a scanning electron microscope (SEM, S-4800, Hitachi) equipped with an energy dispersive X-ray (EDX) spectrometer. The thermal analysis (TGA-DTA) was carried out using a Rigaku TG-DTA-PIMS410/s instrument. The measurements were conducted between 22 and 1400 °C at a heating rate of 10 °C/min. The experiment was performed in an alumina crucible under nitrogen atmosphere. The infrared (IR) spectra were measured in the wavenumber range of 400 - 1800 cm^{-1} using a Perkin Elmer Paragon 1000 PC Fourier spectrometer. The UV-visible diffuse reflectance spectra from 200 to 2000 nm were measured at room-temperature using $BaSO_4$ powder as a reference (100% reflectance) with a Perkin Elmer Lamda-950 UV/VIS/NIR spectrophotometer.

The calculations of the electronic structure based on the density function theory (DFT) were carried out using the Cambridge Serial Total Energy Package (CASTEP) [22] module implemented in Materials Studio software. The crystallographic data (the lattice parameters and the atomic coordinates) obtained in the present paper were used in the input configuration of the calculation process. The cut-off energy E_{cut} of the plane wave base was fixed at 700 eV. The exchange-correlation function was adopted as the generalized gradient approximation (GGA) with the Perdew-Burke-Ernzerhof (PBE) [23] format. A 1×1×1 single cell of $KMgAl(PO_4)_2$ was adopted to present the crystal structure. The Monkhorst-Pack k-point mesh was specified as 7×7×7. The criterion for the self-consistency field (SCF) was the convergence of Eigen energies to within 10^{-6} eV·$atom^{-1}$.

The single-crystal XRD data were collected at room-temperature by an Enraf Nonius Turbo CAD4 diffractometer using monochromatic Mo Kα radiation (λ = 0.7107 Å) and ω/2θ scans. A platelet-shaped single-crystal of $KMgAl(PO_4)_2$ with the dimensions of 0.07×0.18×0.45 mm^3 was used. The unit cell parameters were determined from the refinement of 25 reflections measured in the angular range of 9.2° ≤ θ ≤ 17.6°. A total of 191 reflections were measured in the (-6 ≤ *h*

≤ 6; -1≤ k ≤ 6; -1≤ l ≤ 10) hemisphere (R_{in} = 0.051). Only 166 of them were considered as the observed ones according to the statistical criterion [$I > 2\sigma(I)$]. All the measured intensities were corrected for the Lorentz polarization effect. The absorption corrections were made by the Ref-Delf (XABS2) method [24], leading to the transmission factors of T_{min} = 0.54 and T_{max} = 0.98. The resolution and the refinement of the structure were carried out using the WinGX software package [25]. The structure was solved by the direct methods using the SIR-92 program [26].

To confirm the chemical formula of the crystal resulting from the analysis of the XRD data, a calculation of the distribution charge (CHARDI) was carried out using the Chardi-IT-2015 program [27].

3. Results and discussion

3.1. Material synthesis

The photographs of the prepared materials in the single-crystal and powder forms are shown in Fig. 1. The single crystals are of excellent quality, colorless and platelet-shaped, Fig. 1(a-b). The obtained powder is homogeneous, well sintered, of white color and fine appearance, Fig. 1(c).

3.2. X-ray diffraction

The structure of $KMgAl(PO_4)_2$ was determined from the single-crystal XRD data. During the structure refinement, first, the atomic coordinates were determined for K. Successive refinement of difference Fourier syntheses using SHELXL-97 program [28] allowed us to localize distinctive positions for P, Al and two oxygen atoms, while the Mg atoms have not been identified. For this reason, the examination of the values of the Al-O interatomic distances and the residual electron density imposed the hypothesis of the co-existence of Mg^{2+} and Al^{3+} in the same crystallographic position due to their close ionic radii, $R(Mg^{2+})$ = 0.66 Å and $R(Al^{3+})$ = 0.51 Å for IV-fold oxygen coordination [29]. Considering this hypothesis, a final refinement cycle including atomic coordinates and anisotropic displacement parameters led to the reliability factors of R_1 = 0.056, wR_2 = 0.138 and S = 1.23. The experimental conditions for single-crystal XRD measurements, the structure solution and the refinement are reported in Table 1.

$KMgAl(PO_4)_2$ crystallizes in the trigonal class (space group $P\bar{3}m1 - D^3_{3d}$, No. 164) and its lattice constants are $a = b$ = 5.347(1) Å, c = 7.903(10) Å, $\alpha = \beta$ = 90°, γ = 120° (the number of the formula units in the unit-cell Z = 1), the volume of the unit-cell V is 195.68(9) Å^3 and the calculated density ρ_{calc} is 2.379 g/cm^3. The obtained fractional atomic coordinates (x, y, z) and the equivalent isotropic displacement parameters are listed in Table 2.

Further details on the crystal structure investigations may be obtained from Fachinformationzentrum (FIZ) Karlsruhe, 76344 Eggenstein-Leopoldshafen, Germany on quoting the depository number CSD No. 2067239.

The results on the CHARDI analysis are summarized in Table 3. The CHARDI validation models, with a cationic dispersion factor of 0.1%, and an anionic dispersion factor of 0.4%, validate this structural model. The bond valence sum calculation is in good agreement with the formal oxidation and with the calculated charge $Q(i)$.

The phase purity of the obtained powdered sample was confirmed using powder XRD. The measured powder XRD pattern is shown in Fig.1(c), together with the results of the Rietveld refinement using the WinPLOTR/Fullprof program [30]. The obtained lattice constants, a = 5.347(1) Å, c = 7.903(10) Å and γ = 120° are in good agreement with those determined for the single crystal. The reliability factors are R_p = 7.87; R_{wp} = 13.1 and χ^2 = 4.68 indicating a good compliance between the observed and calculated patterns.

3.3. SEM and EDX

Figure 2 shows the results of the SEM - EDX analysis for the powdered $KMgAl(PO_4)_2$ sample. The surface morphology of this sample is determined by agglomeration of spherical particles, Fig. 2(a). The EDX spectrum presented in Fig. 2(b) confirms the presence of the chemical elements (K, Mg, Al, P and O) constituting the expected composition of $KMgAl(PO_4)_2$. In addition, EDX element maps of the powder were obtained using the EDAX software, Fig. 2(c). The element maps prove that all the above-mentioned elements are uniformly distributed over the studied region of the powdered sample.

3.4. TGA-DTA analysis

Figure 3 shows the results of the TGA-DTA analysis. Upon heating, in the temperature range of 22 – 1400 °C, we observe a weight loss of 3%. The endothermic peak observed at 1179 °C proves the congruent melting of $KMgAl(PO_4)_2$. The cooling curve reveals that the phenomenon is reversible. The two different observed crystallization peaks at 1109, 1072 and 958 °C are attributed to secondary phases appearing after reversible crystallization.

3.5. Crystal structure description

According to the crystallographic analysis, $KMgAl(PO_4)_2$ exhibits a layered structure. It is isostructural to iron phosphates, $KMgFe(PO_4)_2$ [31] and $RbMgFe(PO_4)_2$ [32]. The two-dimensional framework in these materials is built by staking of $[MgM(PO_4)_2]^-$ (where M = Al or Fe) layers along the ***b***-axis, Fig. 4(a-c). Each layer is formed by sharing vertices between the MO_4 (M = 0.5(Al or Fe) + 0.5Mg) and PO_4 tetrahedrons. The structures involve large hexagonal tunnels formed by rings of alternating sharing vertices MO_4 and PO_4 polyhedrons, with alkali metal atoms (K) located inside these tunnels. The tunnels are regular in $KMgAl(PO_4)_2$ and $RbMgFe(PO_4)_2$ and deformed in $KMgFe(PO_4)_2$ and they are oriented along the [001] and [101] directions, respectively, as shown in Fig. 5(a-c).

The interatomic distances and angles in MO_4 (M = Al, Mg), PO_4 and KO_{12} polyhedrons for $KMgAl(PO_4)_2$ are summarized in Table 4. The MO_4 tetrahedrons have three equal M−O distances of 1.808(4) Å and one of 1.795(5) Å. For these tetrahedrons, the M-O bonds are much longer than those (Al-O) observed typically for AlO_4 (1.71 Å) [33, 34] and much shorter than those (Mg-O) for MgO_4 (1.96 Å) [35, 36]. This results in abnormal value of the calculated distribution charge, +2.5 for Mg and Al cations. In addition, such values of M-O distances support the mixing of Mg and Al atoms in the 2*d* sites (Fig.6(a)). The angles O-M-O are between 106.34(1)° (×3) and 112.47(1)° (×3). Similarly, the PO_4 tetrahedrons, (Fig.6(b)), have three P-O distances of 1.512(4) Å and one of 1.509(5) Å, which are comparable to the P-O distance of

1.537 Å suggested by Baur for monophosphates [37] and also agree with the P-O bond lengths varying from 1.502(2) Å to 1.557(2) Å in $KZnAl(PO_4)_2$ and β-$NaZnAl(PO_4)_2$ compounds [19]. The O-P-O bond angles are ranging from 108.42(11)° (×3) to 110.52(12)° (×3). Consequently, the tetrahedral geometry of PO_4 and MO_4 exhibits axial distortion resulting from the corner-sharing PO_4 and MO_4 tetrahedrons. The environment of K consists of 12 oxygen atoms O(2), see Fig.6(c), with K-O(2) distances of 3.168(2) Å in agreement with the limit of the K-O bond length of 3.33 Å suggested by Donnay and Allmann [38].

3.6. Optical characterization

The infrared spectrum of powdered $KMgAl(PO_4)_2$ was shown in figure 7. The IR spectra exhibit all the bands predicted by group theory for The PO_4^{3-} ion of T_d symmetry $(\nu_1)A_1 + (\nu_2)E + 2(\nu_3 + \nu_4)T_2$ [39,40]. Theoretically, only T2(1) and $T_2(2)$ vibrations are the IR-active ones. It is significant to remember that theoretically non-active vibrations can become visible in the IR spectra of solid materials [41]. The obtained spectrum is like those for monophosphates and the assignment of the observed bands to vibration modes was performed following the previous studies [32, 42]. The bands in the range of 1228-1080 cm^{-1} are attributed to antisymmetric triply degenerate P-O stretching mode (ν_3) $T_2(1)$; 1228, 1140 shoulder and 1085 cm^{-1} strong. The asymmetric triply degenerate (ν_4) and symmetric doubly degenerate (ν_2) O-P-O bending modes appear in the ranges of 659-561 cm^{-1}: 659 cm^{-1} strong and 596, 561 shoulder. The week band at 997 cm^{-1} is assigned to symmetric P-O stretching (ν_1) A_1. The symmetric doubly degenerate (ν_2) E O-P-O bending modes and 498-400 cm^{-1}: 498 cm^{-1} shoulder and 462 cm^{-1} strong, respectively. The single observed band corresponding to the symmetric P-O stretching confirms the presence of a single PO_4 group in agreement with the structural study.

The first-principle calculations for the $KMgAl(PO_4)_2$ crystal were performed by the plane-wave pseudopotential method. Figure 8(a) displays the obtained band structure. $KMgAl(PO_4)_2$ is an indirect bandgap semiconductor, as its maximum energy state in the valence band (VB) and its minimum energy state in the conduction band (CB). Both appear at different points of the Brillouin zone as displayed in Fig. 8(b). The calculated energy gap $E_{g,calc}$ for $KMgAl(PO_4)_2$ is 3.34 eV. To verify the DFT calculation results, the UV-visible diffuse reflectance spectra of $KMgAl(PO_4)_2$ were measured; they are shown in Fig. 8(c). The crystal exhibits strong absorption in the range of 200-300 nm due to the Mg|Al-O charge transfer.

The optical bandgap E_g can be determined by the following equations [43,44]:

$$F(R)h\nu = A(h\nu - Eg)^n, \quad (1a)$$

$$F(R) = (1 - R)^2/2R, \quad (1b)$$

where $F(R)$ is the Kubelka-Munk function, A is a constant, R is the reflectivity of the sample, $h\nu$ is the photon energy and $n = 2$ for indirect allowed transitions. From this analysis, we achieve E_g of 3.86 eV, cf. Fig. 8(d), close to the values reported previously for $KZnAl(PO_4)_2$ ($E_g = 3.76$ eV) and β-$NaZnAl(PO_4)_2$ ($E_g = 3.70$ eV) compounds [19]. The optical bandgap for $KMgAl(PO_4)_2$ is slightly higher than the calculated value due to the discontinuity of the exchange correlation energy function [45].

The composition of the calculated energy band structure is further resolved by the total (TDOS) and partial density of states (PDOS), as shown in Fig. 9(a-f). The top of the VB, as well

as the bottom of the CB band mainly originate from the *p*-orbitals of the O^{2-} atoms and the *p*-orbitals of the $Al^{3+}|Mg^{2+}$ atoms, respectively, with a few contributions from the *p*-orbitals of the P^{5+} atoms. In addition, strong hybridizations of the Mg^{2+} and O^{2-} orbitals in the energy range of -10 to 0 eV in the VB suggests strong covalent bonding characteristic of the Mg-O bond.

4. Conclusion

To conclude, a novel aluminophosphate, $KMgAl(PO_4)_2$, was synthesized both by flux growth and sol-gel reaction and its structure was determined by single-crystal X-ray diffraction. The main feature of this compound is a two-dimensional structure with hexagonal tunnels running along the ***c***-axis formed by metal $(Mg|Al)O_4$ and PO_4 tetrahedrons connected by sharing corner oxygen atoms, and alkali metal atoms distributed inside these tunnels. The two-dimensional framework is built by staking of $[MgM(PO_4)_2]^-$ (where M = Al or Fe) layers in the ***a*-*b*** plane, which determines a perfect cleavage feature and a platelet-like shape of the single-crystals. The IR spectrum confirms the structure analysis. The combination of DFT calculation and the UV-visible reflectance measurements indicate that $KMgAl(PO_4)_2$ is an indirect band gap (3.86 eV) semiconductor. The calculation of partial densities of states indicates that the Al|Mg−O groups play the major role in the electron transitions of the studied compound. The layered structure of $KMgAl(PO_4)_2$ is promising for intercalation of sodium and lithium ions in the inter-layer space which will be a source of important ionic conductivity.

Acknowlegments

This work was supported by Spanish Government, Ministry of Science and Innovation (project No. PID2019-108543RB-I00) and by Generalitat de Catalunya (project No. 2017SGR755). This research article has been possible with the support of the Secretaria d'Universitats i Recerca del Departament d'Empresa i Coneixement de la Generalitat de Catalunya, the European Union (UE) and the European Social Fund (ESF) (2020 FI-B 00522).

References

[1] S. Oliver, A. Kuperman, G. A. Ozin, A new model for aluminophosphate formation: Transformation of a linear chain aluminophosphate to chain, layer, and framework structures, Angew. Chem. Int. Ed. 37(1-2) (1998) 46-62.
https://doi.org/10.1002/(SICI)1521-3773(19980202)37:1/2<46::AID-ANIE46>3.0.CO;2-R

[2] J. S. Chen, W. Q. Pang, R. R. Xu, Mixed-bonded open-framework aluminophosphates and related layered materials, Top. Catal. 9(1) (1999) 93-103.
https://doi.org/10.1023/A:1019158405253

[3] R. Nandini Devi, K. Vidyasagar, Solid-state synthesis and characterization of novel aluminophosphates, $A_3Al_2P_3O_{12}$ (A= Na, K, Rb, Tl): influence of A^+ ions on the coordination of aluminum, Inorg. Chem. 39(11) (2000) 2391-2396.
https://doi.org/10.1021/ic991395u

[4] M. Weiss, D. A. Weber, A. Senyshyn, J. Janek, W. G. Zeier, Correlating Transport and Structural Properties in $Li_{1+x}Al_xGe_{2-x}(PO_4)_3$ (LAGP) Prepared from Aqueous Solution, ACS Appl. Mater. Interfaces. 10(13) (2018), 10935-10944.

https://DOI: 10.1021/acsami.8b00842.
[5] Y. Cui, M. M. Mahmoud, M. Rohde, C. Ziebert, H. J. Seifert, Thermal and ionic conductivity studies of lithium aluminum germanium phosphate solid-state electrolyte, Solid State Ionics. 289 (2016) 125-132.
https://doi.org/10.1016/j.ssi.2016.03.007
[6] M. Kotobuki, M. Koishi, Y. Kato, Preparation of $Li_{1.5}Al_{0.5}Ti_{1.5}(PO_4)_3$ solid electrolyte via a co-precipitation method, Ionics. 19(12) (2013) 1945-1948.
https://DOI 10.1007/s11581-013-1000-4
[7] G. Le Flem, (2010), Les Phosphates matériaux pour l'optique. Université de Bordeaux (Université Bordeaux 1), France, 45p.
[8] J. B. Moffat, Phosphates as catalysts, Cat. Rev. Sci. Eng. 18(2) (1978) 199-258. https://doi.org/10.1080/03602457808081868
[9] M. Kacimi, M. Ziyad, F. Hatert, Structural features of $AgCaCdMg_2(PO_4)_3$ and $AgCd_2Mg_2(PO_4)_3$, two new compounds with the alluaudite-type structure, and their catalytic activity in butan-2-ol conversion, Mater. Res. Bull. 40(4) (2005) 682-693.
https://doi.org/10.1016/j.materresbull.2004.12.009
[10] D. Dwibedi, R. Gond, P. Barpanda, Alluaudite $NaCoFe_2(PO_4)_3$ as a 2.9 V cathode for sodium-ion batteries exhibiting bifunctional electrocatalytic activity, Chem. Mater. 31(18) (2019) 7501-7509. https://doi.org/10.1021/acs.chemmater.9b02220
[11] Z. Li, X. Zhao, Influence of excess lithium and sintering on the conductivity of $Li_{1.3}Al_{0.3}Ti_{1.7}(PO_4)_3$, Funct. Mater. Lett. 12(04) (2019) 1950047.
https://doi.org/10.1142/S1793604719500474
[12] M. Wen, H. Wu, S. Cheng, J. Sun, Z. Yang, X. Wu, S. Pan, Experimental characterization and first principles calculations of linear and nonlinear optical properties of two orthophosphates $A_3Al_2(PO_4)_3$ (A= Rb, K), Inorg. Chem. Front. 6(2) (2019) 504-510.
https://doi.org/10.1039/C8QI01249K
[13] I. M. Nagpure, K. N. Shinde, V. Kumar, O. M. Ntwaeaborwa, S. J. Dhoble, H. C. Swart, Combustion synthesis and luminescence investigation of $Na_3Al_2(PO_4)_3$: RE (RE= Ce^{3+}, Eu^{3+} and Mn^{2+}) phosphor, J. Alloys Compd. 492(1-2) (2010) 384-388.
https://doi.org/10.1016/j.jallcom.2009.11.110
[14] M. E. Medina, M. Iglesias, E. Gutierrez-Puebla, M. A. Monge, Solvothermal synthesis and structural relations among three anionic aluminophosphates; catalytic behavior, J. Mater. Chem. 14(5) (2004) 845-850.
doi.org/10.1039/B311618B
[15] O. Yakubovich, G. Kiriukhina, L. Shvanskaya, A. Volkov, O. Dimitrova, Joint crystallization of $KCuAl[PO_4]_2$ and $K(Al, Zn)_2[(P, Si)O_4]_2$: crystal chemistry and mechanism of formation of phosphate-silicate epitaxial heterostructure, Acta Crystallogr., Sect. B. 76(3) (2020) 483-491. https://doi.org/10.1107/S2052520620005715
[16] O. V. Yakubovich, G. V. Kiriukhina, O. V. Dimitrova, E. A. Zvereva, L. V. Shvanskaya, O. S. Volkova, A. N. Vasiliev, An open framework crystal structure and physical properties of $RbCuAl(PO_4)_2$, Dalton Trans. 45(6) (2016) 2598-2604.
https://doi.org/10.1039/C5DT04543F

[17] X. A. Chen, L. Zhao, Y. Li, F. Guo, B. M. Chen, Potassium cobalt aluminum mixed phosphate, $K(Co^{II},Al)_2(PO_4)_2$, Acta Crystallogr., Sect. C. 53(12) (1997) 1754-1756.
https://doi.org/10.1107/S0108270197009906
[18] X. Bu, P. Feng, T. E. Gier, G. D. Stucky, Synthesis and crystal structure of feldspar analogs in beryllosilicate and aluminum–cobalt phosphate systems, Microporous Mesoporous Mater. 23(5-6) (1998) 323-330.
https://doi.org/10.1016/S1387-1811(98)00124-3
[19] H. Wang, L. Geng, Y. J. Wang, H. Y. Lu, C. Y. Meng, Synthesis, characterization, and properties of two new phosphate crystals $MZnAl(PO_4)_2$ (M= Na, K) with 3D framework tunnel structures, J. Alloys Compd. 820 (2020) 153176.
https://doi.org/10.1016/j.jallcom.2019.153176
[20] Y. Ma, N. Li, N. Guan, S. Xiang, H. Song, H. Wang, A novel zeolite-like structure based on zinc and aluminum phosphate synthesized from H_3PO_3-containing gel, Microporous Mesoporous Mater. 94(1-3) (2006) 179-184.
https://doi.org/10.1016/j.micromeso.2006.04.001
[21] O. Yakubovich, G. Kiriukhina, A. Volkov, O. Dimitrova, The rich crystal chemistry of the $AMM'(PO_4)_2$ morphotropic series: $NaZnAl(PO_4)_2$, the first Na representative with a new structure type, Acta Crystallogr., Sect. C. 75(5) (2019) 514-522.
https://doi.org/10.1107/S2053229619004327
[22] S. J. Clark, M. D. Segall, C. J. Pickard, P. J. Hasnip, M. I. J. Probert, K. Refson, M. C. Payne, First principles methods using CASTEP, Zeitschrift Fur Krist. 220 (2005) 567-570.
https://doi.org/10.1524/zkri.220.5.567.65075.
[23] M. Zhou, X. Jiang, C. Li, Z. Lin, J. Yao, Y. Wu, The Double Molybdate $Rb_2Ba(MoO_4)_2$: Synthesis, Crystal Structure, Optical, Thermal, Vibrational Properties, and Electronic Structure, Zeitschrift Für Anorg. Und Allg. Chemie. 641 (2015) 2321-2325.
https://doi.org/10.1002/zaac.201500552.
[24] S. Parkin, B. Moezzi, H. Hope, XABS2: an empirical absorption correction program, J. Appl. Crystallogr. 28 (1995) 53-56.
https://doi.org/10.1107/S0021889894009428
[25] L. J. Farrugia, WinGX and ORTEP for Windows: an update, J. Appl. Crystallogr. 45(4) (2012) 849-854.
https://doi.org/10.1107/S0021889812029111
[26] A. Altomare, G. Cascarano, C. Giacovazzo, A. Guagliardi, A. G. G. Moliterni, M. C. Burla, R. Spagna, A package for crystal structure solution by direct methods and refinement, Universities of Bari, Perugia and Roma, Italy(1997).
[27] M. Nespolo, B. Guillot, CHARDI-2015: charge distribution analysis of non-molecular structures, J. Appl. Crystallogr. 49(1) (2016) 317-321.
http://dx.doi.org/10.1107/S1600576715024814
[28] G. M. Sheldrick, SHELXL-97, program for X-ray crystal structure refinement (1997).
https://doi.org/10.1016/S0076-6879(97)77018-6

[29] R. D. Shannon, Revised effective ionic radii and systematic studies of interatomic distances in halides and chalcogenides, Acta crystallographica section A: crystal physics, diffraction, theoretical and general crystallography. 32(5) (1976) 751-767.
https://doi.org/10.1107/S1600576715024814
[30] T. Roisnel, J. Rodríquez-Carvajal, WinPLOTR: a windows tool for powder diffraction pattern analysis, In Materials Science Forum, (Vol. 378, No. 1 (2001, October) pp. 118-123).
[31] A. Badri, M. Hidouri, M. L. López, M. L.Veiga, A. Wattiaux, M. Ben. Amara, The layered iron phosphate $KMgFe(PO_4)_2$: Crystal structure, Mössbauer spectroscopy and ionic conductivity, Solid State Ionics. 180(36-39) (2009) 1558-1563.
https://doi.org/10.1016/j.ssi.2009.10.012
[32] A. Badri, M. Jabli, A. Wattiaux, M. Ben. Amara, Crystal structure, Mössbauer spectroscopy and dye adsorption properties of a new layered iron phosphate $RbMgFe(PO_4)_2$, J. Mol. Struct. 1167 (2018) 161-168.
https://doi.org/10.1016/j.molstruc.2018.04.062
[33] V. Kahlenberg, Crystal structure of $Ba_8[Al_3O_{10}][AlO_4]$, a novel mixed-anion Ba aluminate related to kilchoanite, Mineral. Mag. 65(04) (2001) 533-541.
https://doi:10.1180/002646101750377551.
[34] M. Kanzaki, X. Xue, Structural Characterization of Moganite-Type $AlPO_4$ by NMR and Powder X-ray Diffraction, Inorg. Chem. 51(11) (2012) 6164-6172.
https://doi:10.1021/ic300167k.
[35] Y. Y. Wang, Y. Mu, Y. J. Sun, J. Y. Li, Two new four-connected zeolite-like magnesium aluminophosphates with intersecting 8-ring channels, RSC advances. 4(99) (2014), 56288-56293. https://DOI: 10.1039/C4RA10950C.
[36] G. Wallez, C. Colbeau-Justin, T. Le Mercier, M. Quarton, F. Robert, Crystal Chemistry and Polymorphism of Potassium–Magnesium Monophosphate, J. Solid State Chem. 136(2) (1998) 175-180.
https://doi:10.1006/jssc.1997.7671.
[37] W. H. Baur, The geometry of polyhedral distortions. Predictive relationships for the phosphate group, Acta Crystallogr., Sect. B. 30(5) (1974) 1195-1215.
https://doi.org/10.1107/S0567740874004560
[38] G. Donnay, R. Allmann, Am. Mineral.: J. Earth and Planet. Mater. 55(5-6) (1970) 1003-1015.
[39] S. A. Brandán, S. B. Díaz, R. C. Picot, E. A. Disalvo, A. B. Altabef, Hydration of inorganic phosphates in crystal lattices and in aqueous solution. Spectrochim. Acta A Mol. Biomol. Spectrosc. 66(4-5) (2007) 1152–1164.
https://doi:10.1016/j.saa.2006.05.029
[40] S. A. Brandán, S. B. Díaz, J. L. González, E. A. Disalvo, A. B. Altabef, Experimental and theoretical study of the hydration of phosphate groups in esters of biological interest. Spectrochim. Acta A Mol. Biomol. Spectrosc. 66(4-5) (2007) 884-897. https://doi:10.1016/j.saa.2006.05.005.

[41] W. Jastrzębski, M. Sitarz, M. Rokita, K. Bułat, Infrared spectroscopy of different phosphates structures. Spectrochim. Acta A Mol. Biomol. Spectrosc. 79(4) (2011) 722-727. https://doi:10.1016/j.saa.2010.08.044
[42] A. Badri, M. Hidouri, A. Wattiaux, M. L. López, M. L. Veiga, M. Ben Amara, Crystal structure, IR and Mössbauer spectroscopy and magnetic properties of $KZnFe(PO_4)_2$ related to the zeolite-ABW like compounds, Mater. Res. Bull. 55 (2014) 61-66.
https://doi.org/10.1016/j.materresbull.2014.04.009
[43] J. Sun, H. Wang, Y. Zhang, Y. Zheng, Z. Xu, R. Liu, Structure and luminescent properties of electrodeposited Eu^{3+}-doped CaF_2 thin films, Thin Solid Films. 562 (2014) 478-484.
https://doi.org/10.1016/j.tsf.2014.04.019.
[44] D. L. Wood, J. Tauc, Weak absorption tails in amorphous semiconductors, Phys. Rev. B. 5 (1972) 3144-3151.
https://doi.org/10.1103/PhysRevB.5.3144.
[45] X. Wang, Z. Zhao, Q. Wu, Y. Li, C. Wang, A. Mao, Y. Wang, Synthesis, structure, and luminescence properties of $SrSiAl_2O_3N_2:Eu^{2+}$ phosphors for light-emitting devices and field emission displays, Dalt. Trans. 44 (2015) 11057-11066.
https://doi.org/10.1039/c5dt00800j.

Table 1. Crystallographic data and structure refinement for a single-crystal of $KMgAl(PO_4)_2$.

Crystal data	
Chemical formula	$KMgAl(PO_4)_2$
Crystal system	trigonal
Space group	$P\bar{3}m1$
$a = b$, c (Å)	5.347(1), 7.903(2)
α, β, γ (°)	90, 90, 120
V (Å^3)	195.68(9)
Z	1
Data collection	
Crystal size (mm^3)	0.7×0.18×0.45
Diffractometer	Enraf Nonius Turbo CAD4
Radiation (Å)	0.71073 (Mo K_α)
Monochromator	Graphite
μ (mm^{-1})	1.29
Scan type	ω/2θ
Scan speed	Variable
$2\theta_{min,\ max}$(°)	2.57 → 26.92
Number of unique reflections; R_{int}	191; 0.0966
Number of observed reflections [$I > 2\sigma(I)$]	166
Miller's indices	$-6 \le h \le 6$, $-1 \le k \le 6$, $-1 \le l \le 10$
F(000)	138
Structure solution	
Intensity corrections	Lorentz-polarisation
Absorption correction Ref –Delf	XABS2
Transmission factors T_{min}, T_{max}	0.54, 0.98
Structure solution	Direct method (SIR-92 program)
Reliability factors	$R_1 = 0.056$, $wR_2 = 0.138$, $S = 1.23$
Number of parameters	20
$(\Delta\rho)_{max}$, $(\Delta\rho)_{min}$ (e·Å^{-3})	0.61, -0.92

Table 2. Fractional atomic coordinates (*x*, *y*, *z*), isotropic or equivalent isotropic displacement parameters U_{iso}*/U_{eq} (Å^2) and site occupancy factors (O.F.) for $KMgAl(PO_4)_2$.

Atom	Wyckoff	Site	*x*	*y*	*z*	U_{iso}*/U_{eq}	O.F.
K	1*a*	-3*m*	1	0	0	0.0321(8)	1
Mg	2*d*	3*m*	2/3	1/3	0.6989(3)	0.0206(7)	0.5
Al	2*d*	3*m*	2/3	1/3	0.6989(3)	0.0206(7)	0.5
P	2*d*	3*m*	2/3	1/3	0.2808(2)	0.0192(7)	1
O1	2*d*	3*m*	2/3	1/3	0.4719(2)	0.0259(14)	1
O2	6*g*	*m*	0.5138(5)	0.0276(2)	0.2138(4)	0.0634(16)	1

Table 3. Charge distribution (CHARDI) and bond-valence-sum (BVS) analysis* of cations and anions in $KMgAl(PO_4)_2$.

Cations	*q*(i)	*Q*(i)	C.N.	ECoN	Anions	*q*(i)	*Q*(i)
K	1.00	0.98	12	12.00	O1	-2.00	-1.90
M	2.50	2.50	4	4.00	O2	-2.00	-2.03
P	5.00	5.00	4	4.00			

*M = (Mg, Al), *q*(i) - formal oxidation number, *Q*(i) - calculated charge, C.N. = coordination number, ECoN - effective coordination number.

Table 4. Selected interatomic distances (Å) and angles (°) for MO_4 (M = Al, Mg), PO_4 and KO_{12} polyhedrons in $KMgAl(PO_4)_2$.

MO_4 (M = Al, Mg)			
M - O1	1.795(5)	O1- M -O2	112.47(1) ×3
M - O2 ×3	1.808(4)	O2- M -O2	106.34(1) ×3
< M -O>	1.806		
PO_4			
P - O1	1.509(5)	O1 – P - O2	110.52(1) ×3
P - O2 ×3	1.512(4)	O2 – P - O2	108.42(1) ×3
<P - O>	1.511		
KO_{12}			
K - O2 ×12	3.168(2)		

Figures captions

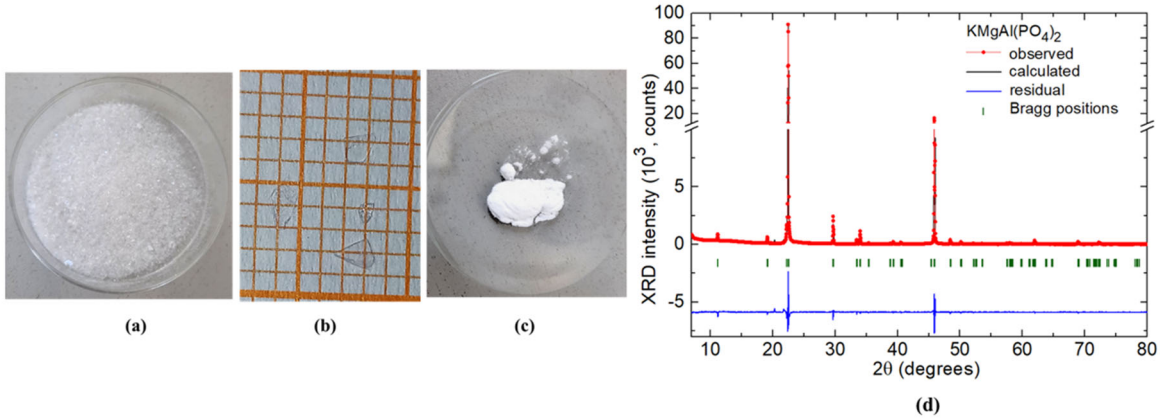

Figure 1. Photographs of $KMgAl(PO_4)_2$ samples: (a) single-crystalline, (b) individual platelet-shaped samples, and (c) well sintered powder. (d) X-ray powder diffraction (XRD) pattern for the powdered sample of $KMgAl(PO_4)_2$ showing the result of the Rietveld refinement: experimental (*black*), calculated (*red*) and residual (*blue*) patterns, *green dashes* – Bragg reflections.

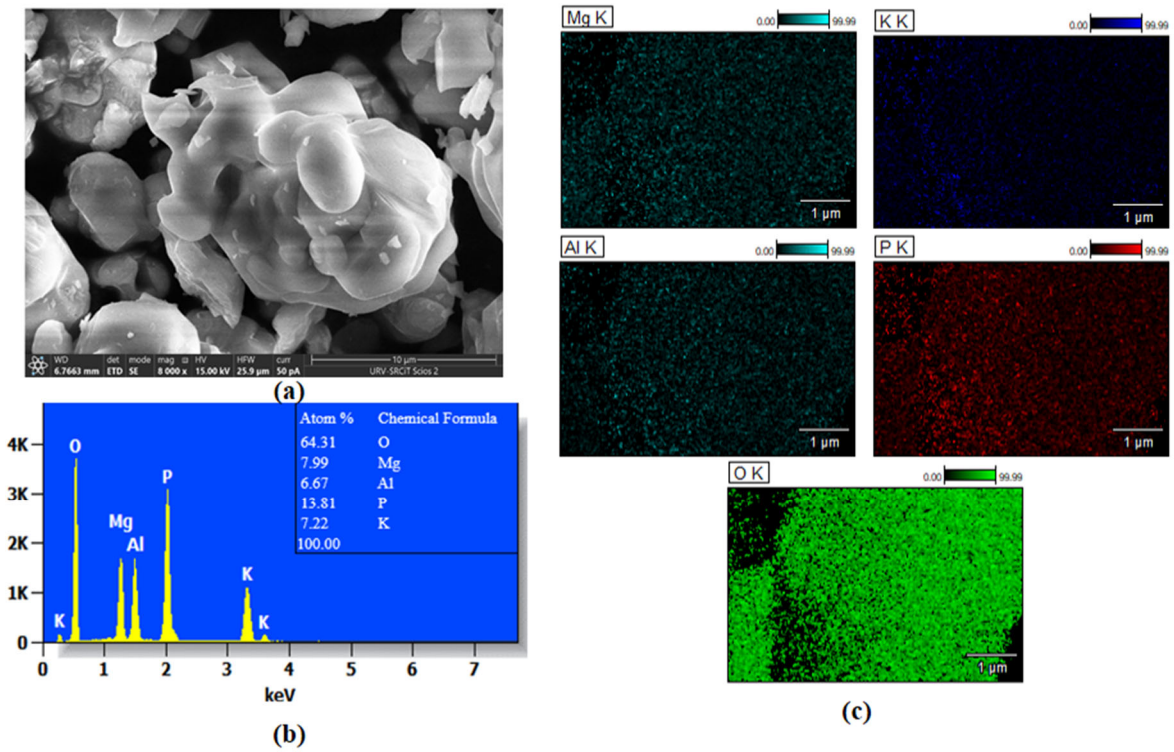

Figure 2. $KMgAl(PO_4)_2$ powder: (a) a typical scanning electron microscope (SEM) image; (b) energy dispersive X-ray (EDX) spectrum, *inset* shows the determined chemical composition.(c) EDX-based element mapping for the $KMgAl(PO_4)_2$ powder: Mg, K, Al, P and O.

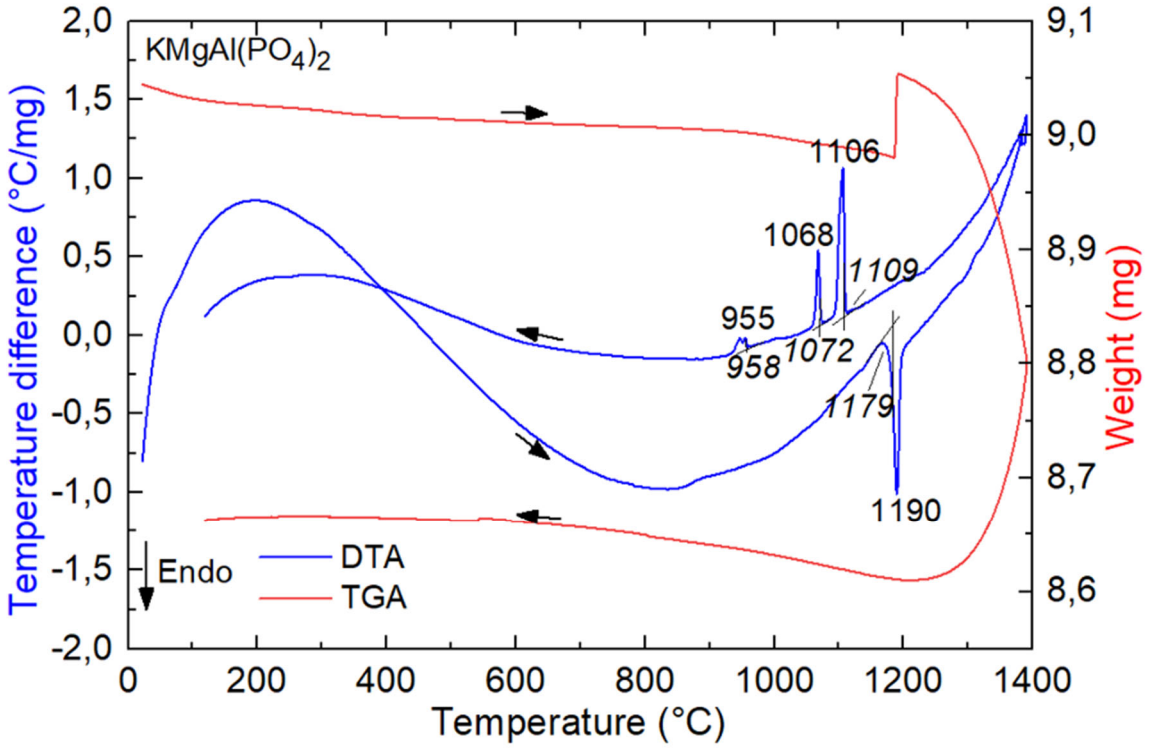

Figure 3. Thermogravimetric analysis (TGA) and differential thermal analysis (DTA) of the powdered $KMgAl(PO_4)_2$ sample.

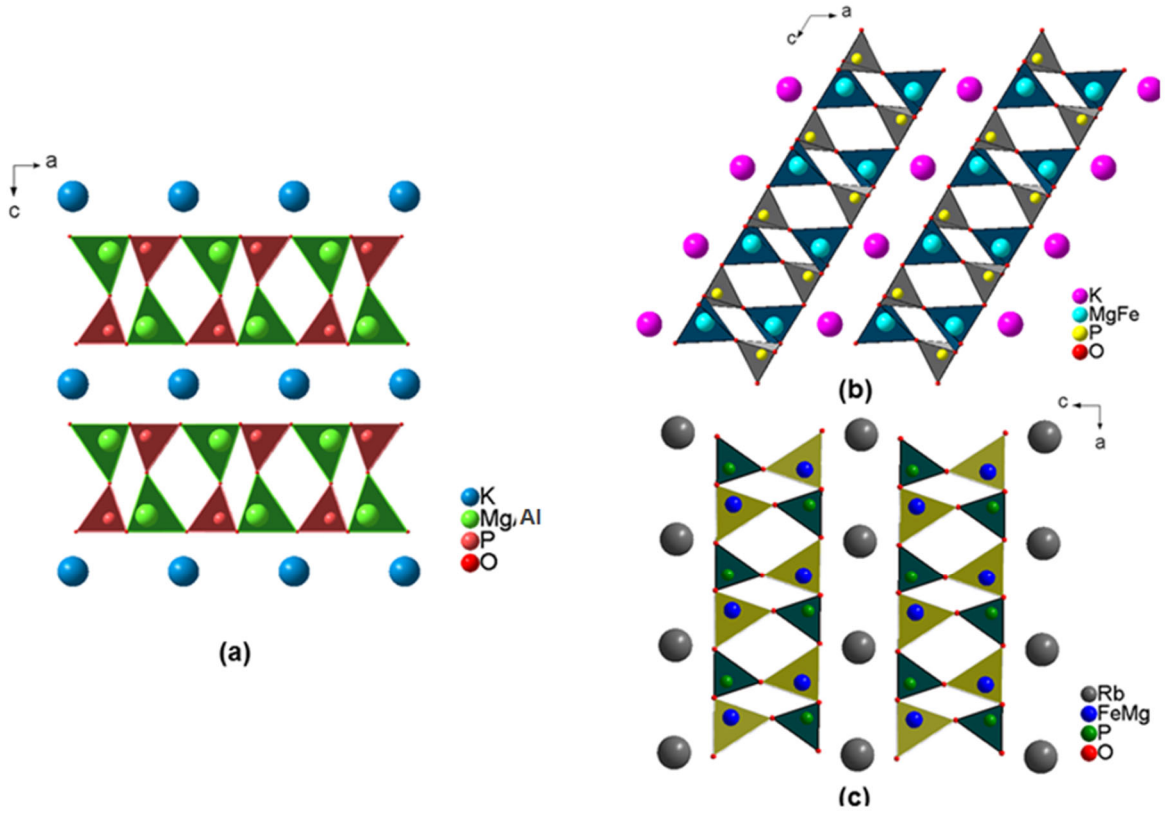

Figure 4. Projections of (a) $KMgAl(PO_4)_2$ (this work) (b) $KMgFe(PO_4)_2$ [31] and (c) $RbMgFe(PO_4)_2$ [32] structures on the ***a*-*c*** plane showing the layered stacking along the ***b***-axis.

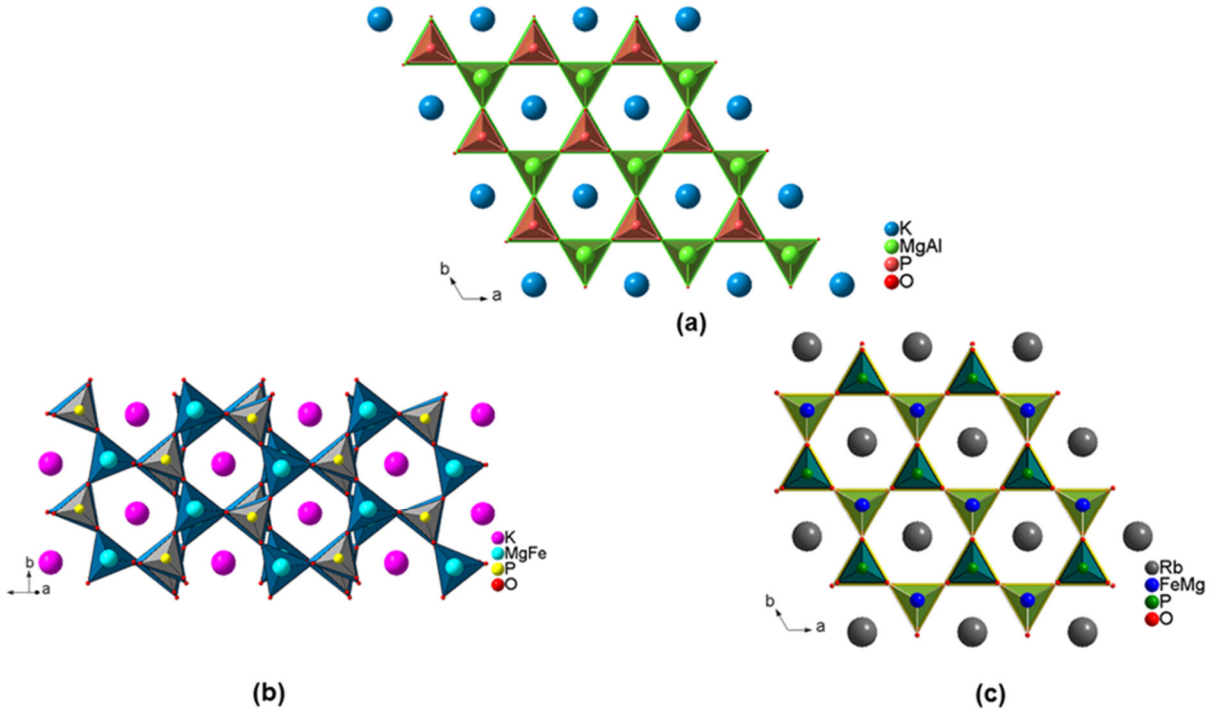

Figure 5. Projections of (a) $KMgAl(PO_4)_2$ (this work) (b) $KMgFe(PO_4)_2$ [31] and (c) $RbMgFe(PO_4)_2$ [32] structures on the ***a-b*** plane showing hexagonal tunnels hosting the alkali metal atoms.

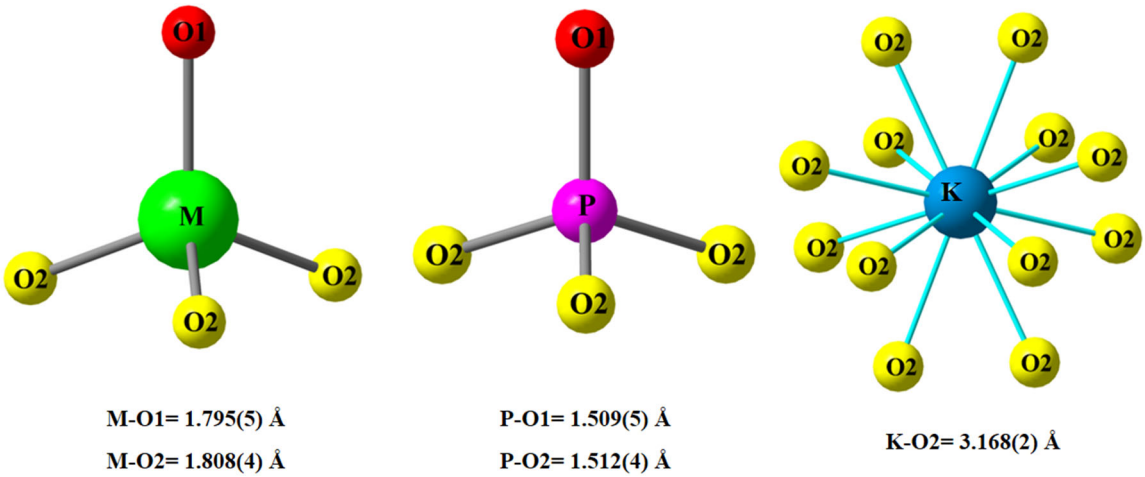

Figure 6. Polyhedra representing the coordination geometries of **(a)** M= (Mg|Al), **(b)** P and **(c)** K in the $KMgAl(PO_4)_2$ structure.

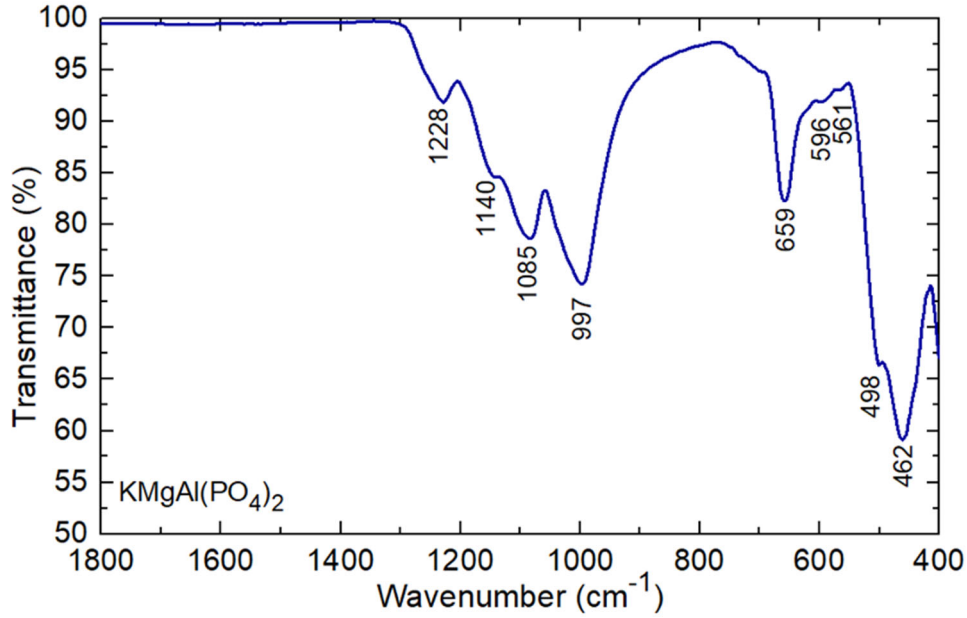

Figure 7. FTIR spectrum of the powdered $KMgAl(PO_4)_2$ sample.

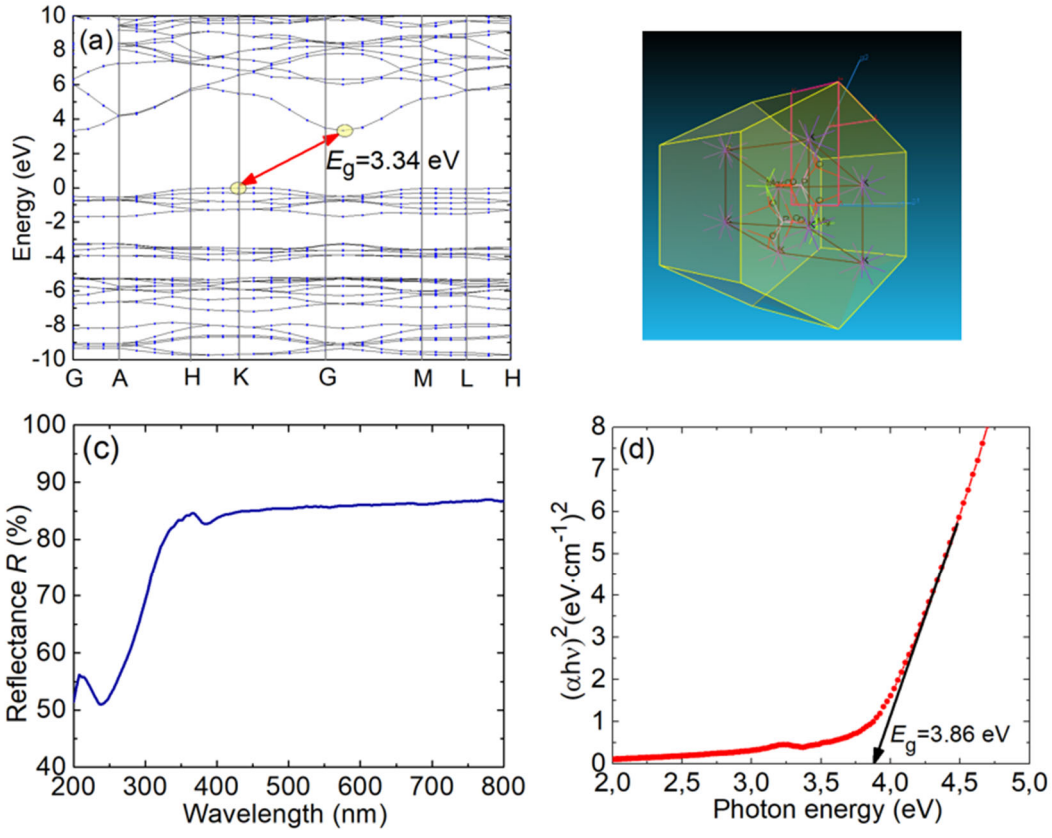

Figure 8. (a) Calculated electronic band structure of $KMgAl(PO_4)_2$; (b) unit-cell and the Brillouin zone of $KMgAl(PO_4)_2$; (c) reflectance spectrum of the powdered $KMgAl(PO_4)_2$ sample; (d) the corresponding Tauc plot.

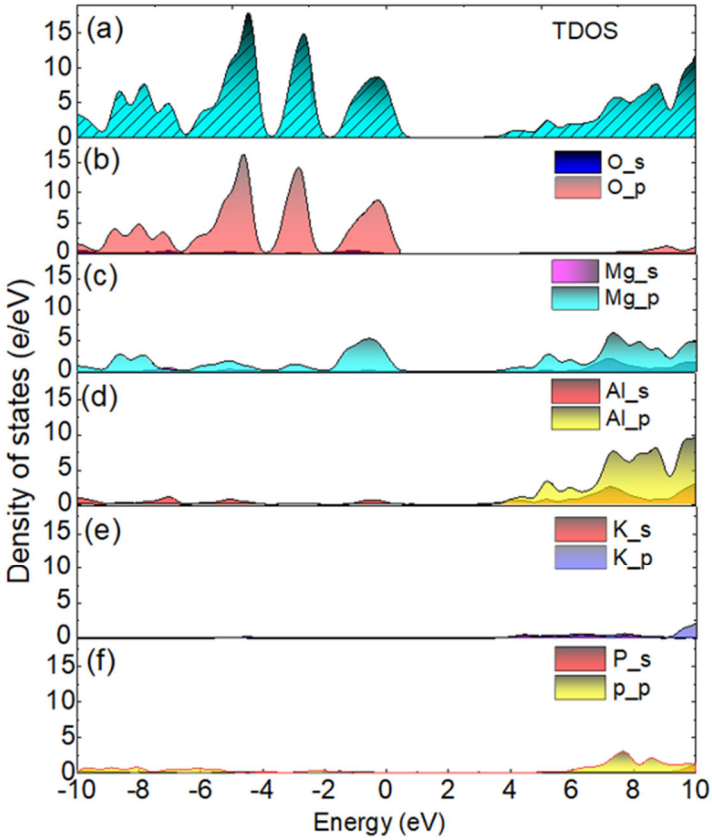

Figure 9. Calculated total (TDOS) and partial (PDOS) densities of states in $KMgAl(PO_4)_2$: (a) TDOS, (b-f) PDOS: (b) O, (c) Mg, (d) Al, (e) K and (f) P.